
Post-Training Second-order Compression for Spiking Neural Networks

Lianfeng Shi¹ Ao Li¹ Benjamin Ward-Cherrier¹

Abstract

Spiking Neural Networks (SNNs) have emerged as a new generation of energy-efficient neural networks suitable for implementation on neuromorphic hardware. As neuromorphic hardware has limited memory and computational resources, parameter pruning and quantization have recently been explored to improve the efficiency of SNNs. State-of-the-art SNN pruning/quantization methods employ multiple compression and training iterations, increasing the cost for pre-trained or very large SNNs. In this paper, we propose a novel one-shot post-training compression framework, Spiking Brain Compression (SBC), that extends the classical Optimal Brain Surgeon method to SNNs. SBC replaces the current-based objective found in the common layer-wise compression method with a spike-train-based objective whose Hessian is cheaply computable, allowing a single backward pass to compress parameters and analytically rescale the rest. Applying SBC to SNN pruning and quantization across event-based and static datasets (up to ImageNet), including SEW-ResNet152 and spike-driven Transformers, we achieve state-of-the-art one-shot post-training compression for SNNs, with single- to double-digit accuracy gains over ANN compression baselines ported to SNNs. We further report a synaptic-operation-based energy proxy and a calibration-size ablation, demonstrating robust performance under sub-one-sample-per-class calibration.

1. Introduction

Spiking Neural Networks (SNNs) have garnered significant attention as a promising power-efficient alternative to traditional Artificial Neural Networks (ANNs). They are composed of spiking neurons that communicate via discrete spikes, analogous to their biological counterparts. This

¹School of Engineering Mathematics and Technology, University of Bristol, England. Correspondence to: Benjamin Ward-Cherrier <b.ward-cherrier@bristol.ac.uk>.

Preprint. January 29, 2026.

sparse, spike-based neural dynamics offers benefits such as low computational power and compatibility with temporal data (Yamazaki et al., 2022), as well as high power efficiency when implemented on neuromorphic chips like True North (Akopyan et al., 2015), Loihi 1 and 2 (Orchard et al., 2021), or SpiNNaker (Furber et al., 2014). However, as these chips have limited computing power and memory, finding ways to improve SNNs’ efficiency on neuromorphic hardware is an important research question (Neil et al., 2016). In this work, we focus on model compression for SNNs, specifically post-training pruning and quantization.

SNN pruning techniques. Several methods for pruning SNNs have emerged in the past five years. UPF (Shi et al., 2024) finds that aggressive unstructured pruning ($\geq 90\%$ sparsity) can yield 10x efficiency increase. (Guo et al., 2020) proposed an unsupervised online pruning technique for SNNs. (Kim et al., 2022) explored the lottery ticket hypothesis (LTH) for SNN and used it as the basis for their unstructured weight pruning method. However, most state-of-the-art (SOTA) SNN pruning methods either require pruning during training or adopt an iterative pruning approach, in which multiple pruning and training iterations are performed. Such approaches are computationally expensive, especially for pre-trained, deep spiking neural networks like SEW-ResNet 152 (Fang et al., 2021a), and Spiking Transformers (Yao et al., 2023; Zhou et al., 2022). With the adoption of transformer architectures for SNNs, the scale of future state-of-the-art SNN models could make retraining costs prohibitively large. Therefore, a more computationally efficient pruning algorithm is urgently needed for the deployment of future next-generation SNNs.

SNN quantization techniques Efforts to apply quantization to SNNs on neuromorphic hardware have recently gained traction. There are two main categories in neural network quantization: Quantization-Aware Training (QAT) and Post Training Quantization (PTQ). QAT allows models to adapt to the quantization through retraining, and there have been several articles written on QAT for SNNs, such as (Lui & Neftci, 2021; Li et al., 2022; Wei et al., 2025). However, PTQ for SNNs is still relatively underdeveloped, especially compared to its ANN counterparts, where the desire to reduce the size of Large Language Models (LLMs) to run on smaller or even edge computing hardware has inspired many algorithms, such as AdaQuant (Jhunjunwala

et al., 2021), Optimal Brain Quantizer (OBQ) (Frantar & Alistarh, 2022), and GPTQ (Frantar et al., 2023).

Other efficiency improvement techniques. Some other notable methods of improving SNN efficiency include knowledge distillation (Xu et al., 2023; Kushawaha et al., 2021), where a larger model is used to train a smaller model, spike rate reduction (Deng et al., 2021; Na et al., 2022; Han & Roy, 2020) and hardware-specific optimizations (Padovano et al., 2024; Fang et al., 2020). Due to space limitations, we do not cover these methods in depth here; they are orthogonal and can be used to complement pruning/quantization, as seen in recent works (Shymyrbay et al., 2023; Chowdhury et al., 2021).

We discovered that the naive application of ANN one-shot post-training compression methods, such as Optimal Brain Compression (Frantar & Alistarh, 2022), to SNNs yields suboptimal results due to a disconnect between ANN methods’ objective functions and SNNs’ layer-wise output spike trains. To address this research gap, we derived an innovative objective function based on the Van Rossum Distance (VRD) (Rossum, 2001) of output spike trains, referred to as the surrogate membrane potential (SMP). By statistically estimating SMP’s Hessian from a calibration dataset, SBC maintains OBC’s computational cost while providing tighter compression guarantees.

Based on SMP, we introduce Spiking Brain Compression, a layer-wise compression algorithm that leverages SMP to compress pre-trained SNNs in one shot. We validate SBC on pruning and quantization tasks with neuromorphic benchmarks and large-scale static datasets, demonstrating efficient, accurate compression of SNNs.

The main contributions of this work can be summarized as follows:

- We formalize a VRD-based loss for layer-wise SNN compression and derive an efficient Hessian that can be sampled from a small calibration dataset.
- We develop *Spiking Brain Compression (SBC)*: a one-shot second-order SNN compression algorithm that supports modern SNN architectures, including deep spiking CNNs and spiking Transformers.
- SBC demonstrates state-of-the-art one-shot post-training SNN compression across neuromorphic and large-scale static benchmarks (up to ImageNet), showing scalability by compressing SEW-ResNet152 (Fang et al., 2021a) and Spike-Driven Transformers (Yao et al., 2023).
- A calibration-size ablation showed stable performance under data-scarce, sub-one-sample-per-class calibration.

2. Preliminary

2.1. Leaky-Integrate-and-Fire (LIF) neuron

We use the discrete LIF neuron model described in (Fang et al., 2021b), with $V_{reset} = 0$. As summarized in Eqs. 1–3, $U[t]$ and $V[t]$ represent the neuron membrane potential after neuron dynamics, and after the trigger of a spike at time t , respectively. $I[t]$ denotes the external input current. $S[t]$ denotes the output spike train. τ_m is the membrane time constant, which governs the rate of decay for the membrane potential.

$$U[t] = \left(1 - \frac{1}{\tau_m}\right) V[t-1] + \frac{1}{\tau_m} I[t] \quad (1)$$

$$S[t] = \Theta(U[t] - V_{th}) \quad (2)$$

$$V[t] = U[t](1 - S[t]) \quad (3)$$

2.2. Optimal Brain Surgeon

Neural network compression methods that use second-order approximation are extensions of the OBS framework (Hasibi & Stork, 1992), which considers the problem of accurately compressing a well-trained dense neural network. We briefly review the OBS rules for selecting the next weight to compress w_p , and the optimal compensation δ_p , given the expected Hessian \mathbf{H} of loss \mathcal{L} :

$$w_p = \underset{w_p}{\operatorname{argmin}} \frac{c_{w_p}^2}{[\mathbf{H}^{-1}]_{pp}}, \delta_p = -\frac{c_{w_p}}{[\mathbf{H}^{-1}]_{pp}} \cdot [\mathbf{H}^{-1}]_{:p} \quad (4)$$

Here, c_{w_p} denotes the changes to weight p (for pruning $c_{w_p} = w_p$, for quantization $c_{w_p} = w_p - \hat{w}_p$ where \hat{w}_p is the nearest quantized expression of w_p). $[\mathbf{H}^{-1}]_{pp}$ denotes the p^{th} diagonal of inverse Hessian, $[\mathbf{H}^{-1}]_{:p}$ is its p^{th} column.

2.2.1. OPTIMAL BRAIN COMPRESSION HESSIAN MATRIX UPDATE

As a weight is pruned, its Hessian matrix $\mathbf{H}' = \mathbf{H}_{-p}$, where \mathbf{H}_{-p} represents matrix \mathbf{H} with row p and column p removed. However, $\mathbf{H}_{-p}^{-1} \neq (\mathbf{H}^{-1})_{-p}$, and calculating the inverse Hessian of the remaining matrix at each pruning iteration can incur a high computational cost. Building upon OBS, Optimal Brain Compression (Frantar & Alistarh, 2022) introduced a straightforward method to obtain the inverse of a Hessian matrix without row p and column p , using the Sherman-Morrison formula:

$$\mathbf{H}_{-p}^{-1} = \left(\mathbf{H}^{-1} - \frac{1}{[\mathbf{H}^{-1}]_{pp}} \mathbf{H}_{:,p}^{-1} \mathbf{H}_{p,:}^{-1}\right)_{-p} \quad (5)$$

3. Methodology

Module-wise compression. Since small current errors accumulate through LIF dynamics, we measure distort-

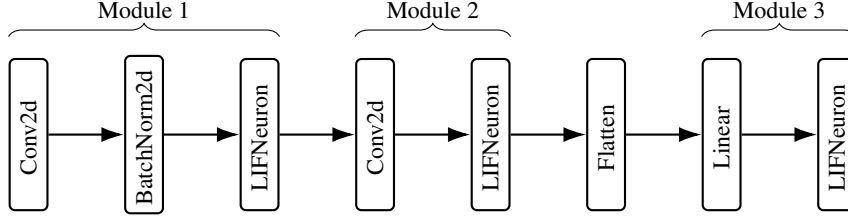


Figure 1. Example SNN modules: each ends with a LIF layer and includes preceding linear/conv/BN layers.

tion at the output spike train. To achieve this, we compress SNNs *module-wise*: Every module comprises Linear/Conv(+BatchNorm) \rightarrow LIF layers; BatchNorm and Conv can be folded into a single linear map, so each module becomes Linear(W) \rightarrow LIF. (Figure 1 visualizes the module concept in an SNN). For an input spike tensor $X \in \{0, 1\}^{T \times d_{in}}$ and weights $W \in \mathbb{R}^{d_{in} \times d_{out}}$, the module produces a spike train $S = f(X, W) \in \{0, 1\}^{T \times d_{out}}$. We treat each module as an independent compression problem.

Problem setup. The goal of module-wise compression is to find a "compressed" W , which we denote \hat{W} , that performs as similarly to the original weights as possible. More formally, the compressed weights \hat{W} should minimize some loss function \mathcal{L} while satisfying some constraints on \hat{W} , expressed as $\mathcal{C}(\hat{W}) > C$:

$$\operatorname{argmin}_{\hat{W}} E_X[\mathcal{L}(f(X, W), f(X, \hat{W}))], \text{ s.t. } \mathcal{C}(\hat{W}) > C \quad (6)$$

The expectation is approximated with N calibration samples.

3.1. Spiking Brain Compression (SBC)

This paper identifies an appropriate loss function \mathcal{L} and computes its expected Hessian H for general SNNs. We refer to this framework as Spiking Brain Compression.

3.1.1. LOSS FUNCTION \mathcal{L}

Let $\hat{S} = f(X, \hat{W})$ and $S = f(X, W)$. Due to the discrete nature of S and \hat{S} , using the squared L2 Norm on $S - \hat{S}$ ignores the time distances between modified and original spikes. To address this, we used the squared VRD between the pre- and post-compression output spike trains as the loss function. Here we represent the VRD decaying exponential kernel $k(t)$ as a function of time constant τ :

$$k[t] = \begin{cases} (1 - \frac{1}{\tau_m})^t \frac{1}{\tau_m} & \text{if } t \geq 0 \\ 0 & \text{if } t < 0 \end{cases} \quad (7)$$

The loss can then be expressed as:

$$\begin{aligned} \mathcal{L}(W) &= VRD(S, \hat{S}) \\ &= \|S(t) * k(t) - \hat{S}(t) * k(t)\|_2^2 \\ &= \|MS - M\hat{S}\|_2^2 \end{aligned} \quad (8)$$

Where the square matrix M of size $d_{time} \times d_{time}$ denotes the convolution matrix of kernel $k(t)$ over d_{time} timesteps. Since the output spike train of an LIF neuron depends solely on its own external input current, and $k(t)$ operates as a convolution along the time dimension, the VRD of each LIF neuron only depends on the weights feeding into the neuron. Consequently, the loss in Eq. 8 can be expressed as the sum of the square VRD of each neuron in the layer.

$$\|MS - M\hat{S}\|_2^2 = \sum_{j=1}^{d_{out}} \|MS_{:,j} - M\hat{S}_{:,j}\|_2^2 \quad (9)$$

Therefore, the Hessian for the synaptic connections of each LIF neuron (i.e., each column of the weight matrix W) can be computed independently, as there are no inter-neuron dependencies. In the following section, we analyze the loss function of an individual neuron, with lower case s , \hat{s} , and w representing the spiketrains and synaptic connections of an individual LIF neuron: $\mathcal{L} = \|Ms - M\hat{s}\|_2^2 = \|Mf(X, w) - Mf(X, \hat{w})\|_2^2$.

3.1.2. SURROGATE MEMBRANE POTENTIAL (SMP)

Here we provide SMP, an approximation of the exact Hessian that is computationally efficient and empirically validated across both small and large SNNs. We first provide the Hessian \mathcal{H} of the loss function \mathcal{L} under the OBS framework. Detailed derivation can be found in Appendix A:

$$\mathcal{H}_{ij} = 2(M \frac{\partial s}{\partial u} x_j)^T M \frac{\partial s}{\partial u} x_i + 2(Ms - M\hat{s})^T M x_i \frac{\partial^2 s}{\partial u^2} x_j \quad (10)$$

Where s and u stand for the layer spike train and layer exact membrane potential, and $\frac{\partial s}{\partial u}$ is the $d_{times} \times d_{times}$ Jacobian, which we name h' , and $\frac{\partial^2 s}{\partial u^2}$ we rename h'' .

We observe that the spike at time t $s[t] = \Theta(u[t] - V_{th})$ (Eq. 2) only depends on the membrane potential at time t . This means h' and h'' are diagonal matrices. Inspired by surrogate gradient (Neftci et al., 2019), we replace the non-differentiable Heaviside function Θ with a differentiable gradient function g , thus h' is a diagonal matrix where $h'_{ii} = g(u_i)$.

There are many different ways to design a surrogate gradient function g , and we intend to explore them in future work.

Currently, we found that a constant function $g(u) = c$, works well for layer-wise compression. g can be seen as a *shallow rectangle surrogate gradient* where every u falls in the active window. Since the OBS framework (Hassibi & Stork, 1992) works with the relative magnitude of the Hessian matrix, c cancels out. Without loss of generality, we set $c = 1$. Let $\mathbf{H} = E_X[H]$ be the expectation of the Hessian over a distribution of input X . With a constant function g , we also obtain $h'' = g' = 0$. We now obtain the Hessian for SMP:

$$\begin{aligned} \mathcal{H}_{SMTij} &= 2(Mh'x_j)^T Mh'x_i = 2(Mx_j)^T Mx_i \\ \mathbf{H}_{SMT} &= E_X[\mathcal{H}_{SMT}] = E_X[2(MX)^T MX] \end{aligned} \quad (11)$$

In fact, \mathbf{H}_{SMT} is the exact Hessian of the least square form $\|MXw - MX\hat{w}\|_2^2$, which is the square L2 Loss on the membrane potential of a spiking neuron with the input current Xw in the absence of spikes.

3.1.3. THE SBC PRUNING ALGORITHM

Here, we introduce a module-wise unstructured pruning framework for SNNs that utilizes SMP. We start by obtaining a per-module pruning target with Layer-Adaptive sparsity for the Magnitude-based Pruning Score (LAMPS) (Lee et al., 2020) to determine per-module pruning percentage from a global pruning target. Appendix C.3 provides a detailed explanation of LAMPS. LAMPS takes $O(d \cdot \log(d))$, where d represents the trainable parameter count in the SNN.

Step 1: Weight ordering. To efficiently determine the pruning order of weights in each module, we record each weight’s loss by performing OBS per neuron with a small batch size B_{in} . Each iteration, we take weights with B_{in} smallest loss according to Eq. 4 and prune them together, then update the inverse Hessian with Woodbury Matrix Identity (Hassibi & Stork, 1992). The per-neuron full algorithm is given in Algorithm 1. For small B_{in} , this takes $O(\frac{d_{in}^3}{B_{in}})$ time and $O(d_{in})$ space.

Algorithm 1 Losses \mathbf{L} for weights \mathbf{w} of neuron with $\mathbf{H}^{-1} = (2(\mathbf{MX})^T \mathbf{MX})^{-1}$, in $O(d_{in}^3/B_{in})$ time.

```

 $\mathbb{M} \leftarrow \{1, \dots, d_{in}\}$ 
 $\mathbf{L} \leftarrow \{\}$ 
for  $i = 1, 1 + B_{in}, \dots, d_{in}$  do
     $s_p \leftarrow \frac{w_p^2}{[\mathbf{H}^{-1}]_{pp}} \quad \forall p \in \mathbb{M}$ 
     $\mathbb{P} \leftarrow$  indices of the  $B_{in}$  smallest  $\{s_p\}_{p \in \mathbb{M}}$ 
     $\mathbf{L}[p] \leftarrow s_p \quad \forall p \in \mathbb{P}$ 
     $\mathbf{w}_{\mathbb{P}} \leftarrow \mathbf{w}_p \quad \forall p \in \mathbb{P}$ 
     $\mathbf{w} \leftarrow \mathbf{w} - \mathbf{H}_{:, \mathbb{P}}^{-1} ((\mathbf{H}^{-1})_{\mathbb{P}})^{-1} \cdot \mathbf{w}_{\mathbb{P}}$ 
     $\mathbf{H}^{-1} \leftarrow \mathbf{H}^{-1} - \mathbf{H}_{:, \mathbb{P}}^{-1} ((\mathbf{H}^{-1})_{\mathbb{P}})^{-1} \mathbf{H}_{\mathbb{P}, :}^{-1}$ 
     $\mathbb{M} \leftarrow \mathbb{M} \setminus \{\mathbb{P}\}$ 
end for
    
```

In actuality, we can batch B_{out} neurons in parallel, given the available GPU resources. This produces a loss for each weight in the module, which we then sort and create a mask \mathbf{M} of pruned weights according to the module pruning target. This takes $O(\frac{d_{out}}{B_{out}} \cdot \frac{d_{in}^3}{B_{in}})$ time and $O(B_{out} \cdot d_{in}^2)$ space.

Step 2: Weight pruning. With a mask \mathbf{M} , we can directly update weights of a neuron according to its local set of weights to remove $\mathbb{P} = \mathbf{M}_{:,i}$ via the group OBS formula $\delta_{\mathbb{P}} = -\mathbf{H}_{:, \mathbb{P}}^{-1} ((\mathbf{H}^{-1})_{\mathbb{P}})^{-1} \mathbf{W}_{:,i}$. This takes $O(\frac{d_{out}}{B_{out}} \cdot d_{in}^3)$ time and $O(B_{out} \cdot d_{in}^2)$ space, but it is generally faster than the weight ordering step.

Algorithm 2 SBC Pruning, with SNN \mathcal{M} , calibration data \mathcal{X} , model sparsity target $s \in [0, 1]$

```

 $\mathbb{M} \leftarrow$  modules( $\mathcal{M}$ ) {get set of modules}
for all  $\mathbf{m} \in \mathbb{M}$  do
     $s_m =$  LAMPS( $\mathcal{M}, s, \mathbf{m}$ ) {module target}
     $\mathbb{X} \leftarrow$  module  $\mathbf{m}$  input data from  $\mathcal{X}, \mathcal{M}$ 
     $\mathbf{H} = \frac{2}{|\mathbb{X}|} \sum_{X \in \mathbb{X}} (MX)^T MX$ 
     $\mathbf{W} \leftarrow$  weights of  $\mathbf{m}$ 
     $\mathbf{L} \leftarrow$  Algorithm 1( $\mathbf{W}, \mathbf{H}^{-1}$ )
     $\mathbf{M} \leftarrow$  indices of  $|\mathbf{W}| \cdot s_m$  smallest  $\mathbf{L}$ 
    for  $i = 1, \dots, d_{out}$  do
         $\mathbb{P} \leftarrow \mathbf{M}_{:,i}$ 
         $\delta_{\mathbb{P}} \leftarrow -\mathbf{H}_{:, \mathbb{P}}^{-1} ((\mathbf{H}^{-1})_{\mathbb{P}})^{-1} \mathbf{W}_{:,i}$ 
         $\mathbf{W}_{:,i} \leftarrow \mathbf{W}_{:,i} + \delta_{\mathbb{P}}$ 
    end for
end for
    
```

Complexity. To summarise, per-module SBC has space complexity $O(B_{out} \cdot d_{in}^2)$ and time complexity $O(\frac{d_{out}}{B_{out}} \cdot \frac{d_{in}^3}{B_{in}})$, with d_{in}, d_{out} refer to the input and output dimension of the linearized parameterized layer in the module. Batch sizes B_{in} and B_{out} are adjusted to balance time and space constraints based on hardware availability.

Modern SNN architectures. SBC can also handle compression of modern SNNs like Spiking ResNets (Fang et al., 2021a) and Spiking Transformer (Zhou et al., 2022; Yao et al., 2023) architectures. Appendix B provides implementation details. The intuition is to treat each module separately, and when two different parameterized layers feed into the same spiking neuron layer, to concatenate the parameterized layers’ weights and inputs.

3.1.4. THE SBC QUANTIZATION ALGORITHM

Quantization is essential to the practical deployment of SNNs on neuromorphic hardware. Mainstream neuromorphic hardware stores parameters in low precision, as part of the hardware design choice and/or to save space. For example, SpiNNaker 2 (optimized for 8- and 16-bit), Tianjic (8-bit), Loihi 1 (9-bit), Loihi 2 (up to 32, but default to

Table 1. Datasets and SNN architectures used for compression. τ_m is the membrane time constant of the LIF neuron layers, and T is the number of timesteps. Note that the SEW-ResNet family uses Integrate-and-Fire (IF) neurons, which are equivalent to LIF neurons with $\tau_m = \infty$.

Dataset	Architecture	Input Shape	τ_m	T	Accuracy(%)
N-MNIST	2FC	34x34x2	2.0	100	98.31
CIFAR10-DVS	4Conv+2FC	64x64x2	2.0	20	71.50
DVS128-Gesture	5Conv+2FC	128x128x2	2.0	20	95.14
ASL-DVS	4Conv+1FC	180x240x2	2.0	30	96.53
CIFAR-100	VGG16SNN	32x32x3	1.33	5	71.05
ImageNet	SEW-ResNets	256x256x3	$+\infty$	4	63.12-69.18
ImageNet	Spike-Driven Transformer	256x256x3	2.0	4	72.28-77.07

8-bit), and BrainScaleS-2 (6-bit) (Furber et al., 2014; Deng et al., 2020; Orchard et al., 2021; Pehle et al., 2022).

Furthermore, prior work (Liu et al., 2023) demonstrated that naive quantization of SNNs performs poorly on neuromorphic hardware. This underscores the need for a robust post-training quantization algorithm, such as ours, to enable large-scale SNN deployment.

The SBC quantization algorithm largely follows GPTQ (Frantar et al., 2023), replacing the layer-wise Hessian with \mathbf{H}_{SMP} . It has per-module space complexity $O(d_{in}^2)$ and time complexity $O(\max\{d_{out} \cdot d_{in}^2, d_{in}^3\})$.

3.2. Comparing SBC with OBC

A naive implementation of OBC for SNNs would use a loss function directly on the linearized layer’s output. It has the Hessian:

$$\mathbf{H}_{OBC} = E_X[\mathcal{H}_{OBC}] = E_X[2X^T X] \quad (12)$$

Recall Eq.11, $M \frac{\partial s}{\partial u} = Mh'$ always preserves the lower triangle structure (for spike trains with spikes) because M is lower triangular, and h' is diagonal. This means the simplification $Mh' = I$, i.e. \mathbf{H}_{OBC} , is typically weaker than keeping M , i.e. \mathbf{H}_{SMT} .

4. Experiments

To explore how SBC works in practice, we performed pruning and quantization on models trained with neuromorphic and static datasets. SNNs can leverage unstructured pruning to reduce compute (Shi et al., 2024) on neuromorphic hardware, unlike ANNs on GPUs. For this reason, the experiments are focused on pruning, while we conducted quantization experiments only on N-MNIST, CIFAR10-DVS, and DVS128-Gesture.

The specifications of each model are listed in Table 1. SNN implementation is based on the SpikingJelly library (Fang et al., 2023). Experiments were conducted on a single Nvidia A4500 (20GB) GPU.

Four models were trained on neuromorphic datasets N-MNIST, DVS128 Gesture, DVS-CIFAR10, and ASL-DVS. N-MNIST was trained on the Adam optimizer with $lr = 0.001$ and a maximum of 200 epochs. DVS-CIFAR10 and DVS128-Gestures were trained on the Adam optimizer with Cosine Annealing $lr = 0.001$, and max epoch 512. ASL-DVS was trained with the SGD optimizer and Cosine Annealing, with $lr = 0.001$ for 90 epochs. N-MNIST, DVS128-Gesture, and ASL-DVS maintained their original size, whereas DVS-CIFAR10 was downsized due to the long training time.

The Spiking VGG16 model was chosen for the CIFAR-100 dataset. It was trained on SGD optimizer for 300 epochs, with steps at 150 and 225, using an initial learning rate of $lr_{initial} = 0.1$. SEW-ResNet family and Spike-Driven Transformer (SDT) model checkpoints were retrieved from their respective GitHub repositories.

4.1. Pruning Result and Analysis

4.1.1. SBC vs ONE-SHOT POST-TRAINING SNN PRUNING ALGORITHMS

We compared the performance of the naive magnitude-based pruning (MBP) shown in LAMPS, the naive ExactOBS (OBC’s pruning algorithm) implementation on SNN, and SBC at different sparsity levels across all datasets. The accuracies are recorded in Fig. 2. Note that all three post-training one-shot methods pruned the same proportion of weights from each module according to LAMPS; the difference is in how each module prunes its weights.

Across neuromorphic benchmarks, SBC substantially outperforms both ExactOBS and LAMPS+MBP as sparsity increases. In particular, while all methods start from the same unpruned accuracy, SBC maintains high accuracy under extreme pruning (e.g., N-MNIST: -1.59% at 97% sparsity compared to ExactOBS’s -45.07%; DVS128: -1.74% at 97% sparsity compared to ExactOBS’s -9.38%), and shows similar robustness on CIFAR10-DVS and ASL-DVS where competing methods degrade more rapidly. In short, SBC

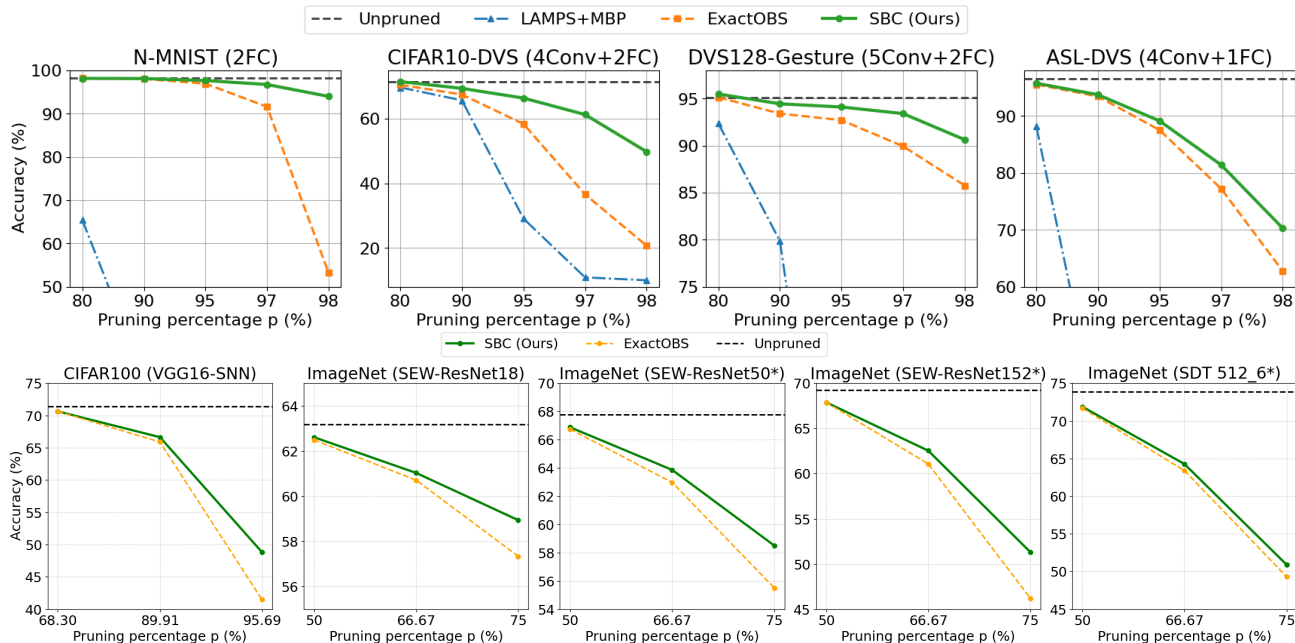


Figure 2. Neuromorphic (top row) and static (bottom row) dataset pruning results, post-training one-shot SNN pruning algorithms. (*) models are the largest SNNs pruned to date. Tables: Appx. D

preserves performance at low sparsity and extends the usable sparsity range relative to other one-shot post-training methods.

The static-dataset results mirror this trend: SBC has the largest gains compared to ExactOBS at very high sparsities (e.g., CIFAR-100 VGG16-SNN: +7.47% at 75% sparsity). On ImageNet across SEW-ResNet variants and Spike-Driven Transformer, SBC consistently matches or improves ExactOBS, demonstrating that SBC is the SOTA one-shot post-training pruning algorithm for SNNs.

4.1.2. SBC VS PAT ALGORITHMS

We compare SBC (with and without post-pruning fine-tuning) against representative PAT baselines, including LTH (Kim et al., 2022), UPF (Shi et al., 2024), and STDS (Chen et al., 2022); accuracy and wall-clock pruning times are reported in Fig. 3. Across CIFAR-100 and ImageNet, SBC reaches competitive accuracy, and adding a short fine-tuning phase further closes the gap to PAT methods while incurring minimal additional computational cost.

Concretely, on CIFAR-100 at 68.30% and 89.91% sparsity, SBC improves top-1 accuracy by 2.02% and 0.06% versus the IMP found in LTH, while reducing pruning time by roughly two orders of magnitude. SBC also outperforms LTH Early Bird methods across the evaluated sparsity targets while running 5–7× faster. On ImageNet, SBC matches or approaches UPF/STDS accuracy but requires substantially less time (three orders of magnitude faster for the

pruning step); with fine-tuning, SBC surpasses UPF’s accuracy but remains slightly below STDS. These results indicate that SBC is a cost-effective alternative to full PAT pipelines: it delivers strong, deployable sparsity with far lower compute and provides flexibility to trade a small additional cost for further accuracy gains.

4.1.3. LARGE SNNs PRUNING

Crucially, the lower computation cost enables SBC to prune large SNNs such as SEW ResNet152 and Spike-Driven Transformer 512.6, when PAT methods become too costly. To the best of our knowledge (Kim et al., 2022; Chen et al., 2022; Shi et al., 2024; Wei et al., 2025), this experiment is the first time SNNs with more than 34 layers have been pruned, the first spiking Transformer trained on ImageNet-scale dataset being pruned, and the first SNNs trained on an ImageNet-scale dataset with more than 19 layers have been pruned (Kim’s experiment on Spiking ResNet-34 (Kim et al., 2022) was trained on Tiny-ImageNet (Le & Yang, 2015)). To the best of our knowledge, SEW-ResNet152 is also the largest and deepest SNN model that has been subjected to unstructured pruning by any algorithm to date. This reaffirms SBC as the SOTA one-shot post-training compression method for SNNs.

In conclusion, the SBC pruning method consistently outperforms current one-shot post-training pruning algorithms for SNNs, achieving one-shot post-training pruning SOTA for SNNs. It is competitive and sometimes even exceeds the accuracy of the SOTA SNN iterative pruning method (Kim

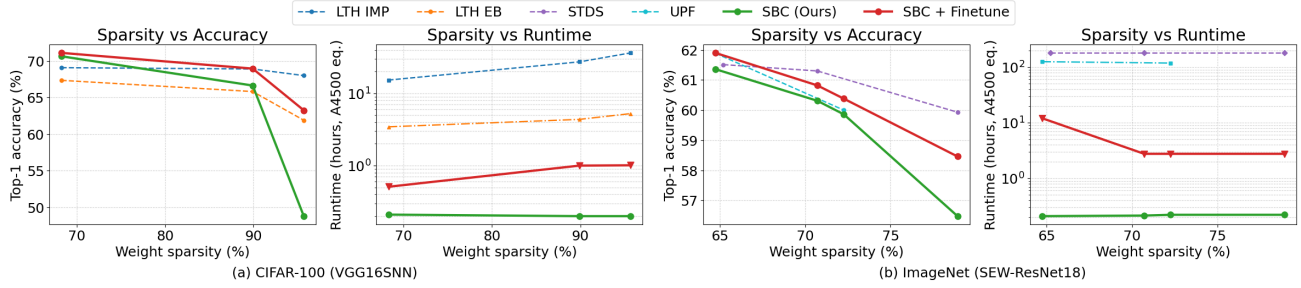


Figure 3. Large static dataset pruning results, SBC (Ours) vs PAT methods. Tables: Appx. D

Table 2. Neuromorphic datasets quantization result

Dataset	Architecture	Time step	Uncompressed Acc. (%)	Top-1 Acc. SBC(Ours) (%)	Top-1 Acc. ExactOBS (%)	Top-1 Acc. RTN (%)	Bit width
N-MNIST	2FC	100	98.31	98.14	98.16	97.58	4-bit
				97.81	97.33	62.26	3-bit
				92.40	64.29	20.34	2-bit
CIFAR10-DVS	4Conv+2FC	20	71.50	69.96	70.30	66.40	4-bit
				69.64	67.56	52.70	3-bit
				60.70	59.40	20.50	2-bit
DVS128-Gesture	5Conv+2FC	20	95.14	87.43	86.67	87.15	4-bit
				81.88	81.25	78.47	3-bit
				64.79	62.78	53.82	2-bit

et al., 2022), with 1 to 3 orders of magnitude of time savings.

4.2. Quantization Result and Analysis

We compared SBC’s quantization accuracy with a baseline method and vanilla implementation of GPTQ (Frantar et al., 2023), the state-of-the-art quantization derivative of OBC, on SNN. The quantization experiment used the same trained models and sample data as the pruning experiment. The models were quantized to 4, 3, and 2 bit widths.

This work used the GPTQ framework for quantization experiments. GPTQ quantizes each linear/convolution ANN layer according to standard uniform per-channel symmetric quantization on the min-max grid, similar to (Dettmers et al., 2022). We chose a symmetric quantization grid for the low computing cost when deploying to neuromorphic hardware. The weights are then quantized in the ascending diagonal inverse Hessian order, resulting in a quantization order from largest to smallest loss on an equal-spacing quantization grid, according to Eq. 4. The quantization grids and weight order are the same as GPTQ. It is notable that SBC quantization can be applied to arbitrary quantization grids.

The baseline method, which Rounds each weight To its Nearest quantized target value, is called RTN. Note that all three methods (RTN, vanilla GPTQ, and SBC) share the same quantization grid, which means all three methods

have precisely the same set of quantization target values to round to, and the difference in accuracy only comes from the choice of target. The result of the quantization experiment can be found in Table 2. Each quantization result is computed as the average of 5 runs using randomly selected sample datasets.

SBC’s performance is generally better than that of RTN and GPTQ. It can quantize the CIFAR10-DVS model to 3-bit precision with a 1.86% drop in accuracy. However, SBC does not consistently outperform RTN and GPTQ in higher-precision quantization for CIFAR10-DVS and DVS128-Gesture. This is caused by the weight compensation, which pushes later-quantized weights to more extreme values. These extreme values are outside of the range of the quantization grid. Nevertheless, SBC achieves the best quantization result among the three methods at the lowest bit representation tested (2bit), outperforming the next-best method by 28.11%, 1.30%, and 2.01%, respectively.

4.3. Efficiency Estimation with SOPs

We use synaptic operations (SOPs) (Shi et al., 2024) as a proxy metric to estimate the energy consumption of an SNN on neuromorphic hardware. This is supported by (Basu et al., 2022), a detailed review of existing neuromorphic hardware. In Table 3, we provide average SOPs for 4Conv-2FC trained

on CIFAR10-DVS, VGGsNN-16 trained on CIFAR-100, and SEW-ResNet18 trained on ImageNet at different sparsities. These results demonstrated SBC’s effectiveness in reducing SOPs while maintaining model accuracy.

Table 3. Synaptic operations per forward pass at different sparsity levels.

Dataset / Model	Sparsity (%)	SOPs (M)	Accuracy (%)
CIFAR10-DVS	0	119.2	71.50
4CONV+2FC	90	25.51	69.40
CIFAR-100	0	107.95	71.05
VGGsNN-16	89.91	35.85	68.96
ImageNet	0	1134.40	63.18
SEW-ResNet18	72.26	697.24	60.38

4.4. Ablation on Calibration Data Size

We evaluated SBC under varying calibration-set sizes on three models: 4Conv2FC on CIFAR-10-DVS, VGGsNN-16 on CIFAR-100, and SEW-ResNet18 on ImageNet. For each setting, we drew three independent stratified calibration datasets of the indicated size, applied SBC using only these samples, and reported the mean and standard deviation of the resulting test accuracy. Calibration size in Table 4 denotes the absolute size of the calibration dataset.

Table 4. Classification accuracy at different calibration dataset sizes for each dataset/model pair.

Dataset / Model	Calibr. size	Accuracy (%)
CIFAR10-DVS 4CONV+2FC	10	49.64 (± 1.27)
	90	61.90 (± 0.21)
	900	63.84 (± 0.49)
	9000	64.04 (± 0.35)
CIFAR-100 VGGsNN-16	100	62.19 (± 0.43)
	1000	65.80 (± 0.07)
	10000	66.42 (± 0.17)
ImageNet SEW-ResNet18	100	49.35 (± 0.19)
	1000	55.06 (± 0.12)
	10000	55.89 (± 0.11)
	50000	55.89 (± 0.04)

These results show that SBC already achieves strong accuracy on the neuromorphic dataset with only 90 calibration samples per class, and on the static datasets with as few as 1–10 samples per class. Interestingly, for SEW-ResNet18 on ImageNet, even 100 calibration images (0.1 images/class) yield competitive performance. In all but one case, the standard deviations are $\leq 0.5\%$, demonstrating SBC’s robustness against the size of the calibration set.

5. Discussion

We have identified two limitations of SBC that will be a significant part of the future work. First, in quantization experiments, we observed the out-of-bounds problem with the min-max quantization grid. A study on the relationship between the choice of the quantization grid and quantization performance is needed. Secondly, we aim to explore more sophisticated surrogate gradients g' and M , or even a general $d_{time} \times d_{times}$ matrix in place of M in the current H_{SMP} . These matrices can be adjusted depending on each neuron’s properties that are not expected to change during compression, such as spike rates. However, we would like to note that a naive implementation of custom Hessian matrices for each output would have high space complexity $\Theta(d_{out} \cdot d_{in}^2)$. In the conv2 layer of the last blocks in the SEW-ResNet152, which has linearized $d_{in} = 4608$ and $d_{out} = 512$, the Hessian would take up $512 \times 4608^2 \times 4bit = 43.5GB$ of space at fp32. As SNN architectures scale, this cost grows quickly, making a lower-complexity strategy essential for practical compression use cases.

6. Conclusion

In conclusion, this paper proposes a one-shot, efficient, post-training compression framework for SNNs, utilizing a second-order approximation of the per-layer spike train loss to dynamically compress and compensate for the compression. Through empirical analysis, this paper shows SBC’s effectiveness in compressing SNNs trained on neuromorphic and static datasets, outperforming current SOTA on SNN post-training one-shot methods, and being competitive with the accuracy of iterative retraining compression methods while providing a 1-2 orders of magnitude decrease in compression time. We expect this work to pave the way for the efficient compression of very large SNNs, such as deep SNNs and spiking Transformers, for low-power, edge computing, and robotic use cases.

Impact Statement

This paper presents work whose goal is to advance the field of Machine Learning. There are many potential societal consequences of our work, none of which we feel must be specifically highlighted here.

References

Akopyan, F., Sawada, J., Cassidy, A., Alvarez-Icaza, R., Arthur, J., Merolla, P., Imam, N., Nakamura, Y., Datta, P., Nam, G.-J., Taba, B., Beakes, M., Brezzo, B., Kuang, J. B., Manohar, R., Risk, W. P., Jackson, B., and Modha, D. S. Truenorth: Design and tool flow of a 65 mw 1

- million neuron programmable neurosynaptic chip. *IEEE Transactions on Computer-Aided Design of Integrated Circuits and Systems*, 34(10):1537–1557, 2015.
- Basu, A., Deng, L., Frenkel, C., and Zhang, X. Spiking neural network integrated circuits: A review of trends and future directions. In *2022 IEEE custom integrated circuits conference (CICC)*, pp. 1–8. IEEE, 2022.
- Chen, Y., Yu, Z., Fang, W., Ma, Z., Huang, T., and Tian, Y. State transition of dendritic spines improves learning of sparse spiking neural networks. In Chaudhuri, K., Jegelka, S., Song, L., Szepesvari, C., Niu, G., and Sabato, S. (eds.), *Proceedings of the 39th International Conference on Machine Learning*, volume 162 of *Proceedings of Machine Learning Research*, pp. 3701–3715. PMLR, 17–23 Jul 2022. URL <https://proceedings.mlr.press/v162/chen22ac.html>.
- Chowdhury, S. S., Garg, I., and Roy, K. Spatio-temporal pruning and quantization for low-latency spiking neural networks. In *2021 International Joint Conference on Neural Networks (IJCNN)*, pp. 1–9. IEEE, 2021.
- Deng, L., Wang, G., Li, G., Li, S., Liang, L., Zhu, M., Wu, Y., Yang, Z., Zou, Z., Pei, J., Wu, Z., Hu, X., Ding, Y., He, W., Xie, Y., and Shi, L. Tianjic: A unified and scalable chip bridging spike-based and continuous neural computation. *IEEE Journal of Solid-State Circuits*, 55(8): 2228–2246, 2020. doi: 10.1109/JSSC.2020.2970709.
- Deng, L., Wu, Y., Hu, Y., Liang, L., Li, G., Hu, X., Ding, Y., Li, P., and Xie, Y. Comprehensive snn compression using admm optimization and activity regularization. *IEEE transactions on neural networks and learning systems*, 34(6):2791–2805, 2021.
- Dettmers, T., Lewis, M., Belkada, Y., and Zettlemoyer, L. Gpt3. int8 (): 8-bit matrix multiplication for transformers at scale. *Advances in neural information processing systems*, 35:30318–30332, 2022.
- Fang, H., Mei, Z., Shrestha, A., Zhao, Z., Li, Y., and Qiu, Q. Encoding, model, and architecture: systematic optimization for spiking neural network in fpgas. In *Proceedings of the 39th International Conference on Computer-Aided Design, ICCAD '20*, New York, NY, USA, 2020. Association for Computing Machinery.
- Fang, W., Yu, Z., Chen, Y., Huang, T., Masquelier, T., and Tian, Y. Deep residual learning in spiking neural networks. *Advances in Neural Information Processing Systems*, 34:21056–21069, 2021a.
- Fang, W., Yu, Z., Chen, Y., Masquelier, T., Huang, T., and Tian, Y. Incorporating learnable membrane time constant to enhance learning of spiking neural networks. In *Proceedings of the IEEE/CVF international conference on computer vision*, pp. 2661–2671, 2021b.
- Fang, W., Chen, Y., Ding, J., Yu, Z., Masquelier, T., Chen, D., Huang, L., Zhou, H., Li, G., and Tian, Y. Spikingjelly: An open-source machine learning infrastructure platform for spike-based intelligence. *Science Advances*, 9(40): eadi1480, 2023.
- Frantar, E. and Alistarh, D. Optimal brain compression: A framework for accurate post-training quantization and pruning. *Advances in Neural Information Processing Systems*, 35:4475–4488, 2022.
- Frantar, E., Ashkboos, S., Hoefler, T., and Alistarh, D. Gptq: Accurate post-training quantization for generative pre-trained transformers, 2023.
- Furber, S. B., Galluppi, F., Temple, S., and Plana, L. A. The spinnaker project. *Proceedings of the IEEE*, 102(5): 652–665, 2014.
- Guo, W., Fouda, M. E., Yantir, H. E., Eltawil, A. M., and Salama, K. N. Unsupervised Adaptive Weight Pruning for Energy-Efficient Neuromorphic Systems. *Frontiers in Neuroscience*, Volume 14 - 2020, 2020. ISSN 1662-453X.
- Han, B. and Roy, K. Deep spiking neural network: Energy efficiency through time based coding. In Vedaldi, A., Bischof, H., Brox, T., and Frahm, J.-M. (eds.), *Computer Vision – ECCV 2020*, pp. 388–404, Cham, 2020. Springer International Publishing.
- Hassibi, B. and Stork, D. Second order derivatives for network pruning: Optimal brain surgeon. In Hanson, S., Cowan, J., and Giles, C. (eds.), *Advances in Neural Information Processing Systems*, volume 5. Morgan-Kaufmann, 1992.
- Hu, Y., Tang, H., and Pan, G. Spiking deep residual networks. *IEEE Transactions on Neural Networks and Learning Systems*, 34(8):5200–5205, 2023. doi: 10.1109/TNNLS.2021.3119238.
- Jhunjunwala, D., Gadhikar, A., Joshi, G., and Eldar, Y. C. Adaptive quantization of model updates for communication-efficient federated learning. In *ICASSP 2021-2021 IEEE International Conference on Acoustics, Speech and Signal Processing (ICASSP)*, pp. 3110–3114. IEEE, 2021.
- Kim, Y., Li, Y., Park, H., Venkatesha, Y., Yin, R., and Panda, P. Exploring lottery ticket hypothesis in spiking neural networks. In *European Conference on Computer Vision*, pp. 102–120. Springer, 2022.

- Kushawaha, R. K., Kumar, S., Banerjee, B., and Velmugan, R. Distilling spikes: Knowledge distillation in spiking neural networks. In *2020 25th International Conference on Pattern Recognition (ICPR)*, pp. 4536–4543. IEEE, 2021.
- Le, Y. and Yang, X. S. Tiny imagenet visual recognition challenge. 2015. URL <https://api.semanticscholar.org/CorpusID:16664790>.
- Lee, J., Park, S., Mo, S., Ahn, S., and Shin, J. Layer-adaptive sparsity for the magnitude-based pruning. *arXiv preprint arXiv:2010.07611*, 2020.
- Li, C., Ma, L., and Furber, S. Quantization framework for fast spiking neural networks. *Frontiers in Neuroscience*, 16:918793, 2022.
- Liu, S., Mohammadi, N., and Yi, Y. Quantization-aware training of spiking neural networks for energy-efficient spectrum sensing on loihi chip. *IEEE Transactions on Green Communications and Networking*, 8(2):827–838, 2023.
- Lui, H. W. and Neftci, E. Hessian aware quantization of spiking neural networks. In *International Conference on Neuromorphic Systems 2021*, pp. 1–5, 2021.
- Na, B., Mok, J., Park, S., Lee, D., Choe, H., and Yoon, S. Autosnn: Towards energy-efficient spiking neural networks. In *International conference on machine learning*, pp. 16253–16269. PMLR, 2022.
- Neftci, E. O., Mostafa, H., and Zenke, F. Surrogate gradient learning in spiking neural networks: Bringing the power of gradient-based optimization to spiking neural networks. *IEEE Signal Processing Magazine*, 36(6):51–63, 2019.
- Neil, D., Pfeiffer, M., and Liu, S.-C. Learning to be efficient: algorithms for training low-latency, low-compute deep spiking neural networks. In *Proceedings of the 31st Annual ACM Symposium on Applied Computing, SAC '16*, pp. 293–298, New York, NY, USA, 2016. Association for Computing Machinery.
- Orchard, G., Frady, E. P., Rubin, D. B. D., Sanborn, S., Shrestha, S. B., Sommer, F. T., and Davies, M. Efficient neuromorphic signal processing with loihi 2. In *2021 IEEE Workshop on Signal Processing Systems (SiPS)*, pp. 254–259. IEEE, 2021.
- Padovano, D., Carpegna, A., Savino, A., and Di Carlo, S. Spikeexplorer: Hardware-oriented design space exploration for spiking neural networks on fpga. *Electronics*, 13(9), 2024.
- Pehle, C., Billaudelle, S., Cramer, B., Kaiser, J., Schreiber, K., Stradmann, Y., Weis, J., Leibfried, A., Müller, E., and Schemmel, J. The brainscales-2 accelerated neuromorphic system with hybrid plasticity. *Frontiers in Neuroscience*, 16:795876, 2022.
- Rossum, M. C. W. v. A novel spike distance. *Neural Computation*, 13(4):751–763, 2001.
- Shi, X., Ding, J., Hao, Z., and Yu, Z. Towards energy efficient spiking neural networks: An unstructured pruning framework. In *The Twelfth International Conference on Learning Representations*, 2024.
- Shymyrbay, A., Fouda, M. E., and Eltawil, A. Low precision quantization-aware training in spiking neural networks with differentiable quantization function. In *2023 International Joint Conference on Neural Networks (IJCNN)*, pp. 1–8. IEEE, 2023.
- Wei, W., Zhang, M., Zhou, Z., Belatreche, A., Shan, Y., Liang, Y., Cao, H., Zhang, J., and Yang, Y. Qp-snn: Quantized and pruned spiking neural networks. *arXiv preprint arXiv:2502.05905*, 2025.
- Xu, Q., Li, Y., Shen, J., Liu, J. K., Tang, H., and Pan, G. Constructing deep spiking neural networks from artificial neural networks with knowledge distillation. In *Proceedings of the IEEE/CVF Conference on Computer Vision and Pattern Recognition*, pp. 7886–7895, 2023.
- Yamazaki, K., Vo-Ho, V.-K., Bulsara, D., and Le, N. Spiking neural networks and their applications: A review. *Brain Sciences*, 12(7), 2022.
- Yao, M., Hu, J., Zhou, Z., Yuan, L., Tian, Y., Xu, B., and Li, G. Spike-driven transformer. *Advances in neural information processing systems*, 36:64043–64058, 2023.
- Zhou, Z., Zhu, Y., He, C., Wang, Y., Yan, S., Tian, Y., and Yuan, L. Spikformer: When spiking neural network meets transformer. *arXiv preprint arXiv:2209.15425*, 2022.
- Zhou, Z., Che, K., Fang, W., Tian, K., Zhu, Y., Yan, S., Tian, Y., and Yuan, L. Spikformer v2: Join the high accuracy club on imagenet with an snn ticket. *arXiv preprint arXiv:2401.02020*, 2024.

A. Deriving exact Hessian for individual LIF neuron

We derive the first-order derivative of loss function \mathcal{L} against weight w_i :

$$\begin{aligned}\frac{\partial \mathcal{L}}{\partial w_i} &= \frac{\partial \mathcal{L}}{\partial s} \frac{\partial s}{\partial w_i} = \frac{\|Ms - M\hat{s}\|_2^2}{\partial s} \frac{\partial s}{\partial w_i} \\ &= 2(Ms - M\hat{s})^T M \frac{\partial s}{\partial w_i}\end{aligned}\quad (13)$$

As is customary in OBS framework, with a well-trained neural network, we assume $\nabla_{w_j} \mathcal{L} = 0$ for all weights w_i . Now we can get the second-order derivative:

$$\begin{aligned}\mathcal{H}_{ij} &= \frac{\partial^2 \mathcal{L}}{\partial w_i \partial w_j} \\ &= \frac{\partial}{\partial w_j} (2(Ms - M\hat{s})^T M \frac{\partial s}{\partial w_i}) \quad (\text{by (13)}) \\ &= 2 \left[\frac{\partial}{\partial w_j} (a^T b) \right] \quad \text{where } a = (Ms - M\hat{s}), b = M \frac{\partial s}{\partial w_i} \\ &= 2 \left[\left(\frac{\partial a}{\partial w_j} \right)^T b + a^T \left(\frac{\partial b}{\partial w_j} \right) \right] \quad (\text{product rule}) \\ &= 2 \left[\left(\frac{\partial (Ms - M\hat{s})}{\partial w_j} \right)^T M \frac{\partial s}{\partial w_i} + (Ms - M\hat{s})^T M \frac{\partial^2 Ms}{\partial w_i \partial w_j} \right] \quad \text{expand a and b} \\ &= 2 \left[\left(\frac{\partial (Ms)}{\partial w_j} \right)^T M \frac{\partial s}{\partial w_i} + (Ms - M\hat{s})^T M \frac{\partial^2 s}{\partial w_i \partial w_j} \right] \\ &= 2 \left(M \frac{\partial s}{\partial w_j} \right)^T M \frac{\partial s}{\partial w_i} + 2(Ms - M\hat{s})^T M \frac{\partial^2 s}{\partial w_i \partial w_j}\end{aligned}\quad (14)$$

We can further derive $\frac{\partial s}{\partial w_i}$ and $\frac{\partial^2 s}{\partial w_i \partial w_j}$:

$$\begin{aligned}\frac{\partial s}{\partial w_i} &= \frac{\partial s}{\partial u} \frac{\partial u}{\partial w_i} = \frac{\partial s}{\partial u} x_i \\ \frac{\partial^2 s}{\partial w_i \partial w_j} &= \frac{\partial}{\partial w_j} \left(\frac{\partial s}{\partial u} x_i \right) = x_i \frac{\partial}{\partial w_j} \left(\frac{\partial s}{\partial u} \right) = x_i \left[\frac{\partial}{\partial u} \left(\frac{\partial s}{\partial u} \right) \right] \frac{\partial u}{\partial w_j} = x_i \frac{\partial^2 s}{\partial u^2} x_j\end{aligned}\quad (15)$$

Where x_i, x_j denotes time-varying pre-synaptic spike trains to synaptic connections w_i and w_j , i.e. $x_i = X_{:,i}$. We can now further simplify the exact Hessian Eq. 14:

$$\mathcal{H}_{ij} = 2 \left(M \frac{\partial s}{\partial u} x_j \right)^T M \frac{\partial s}{\partial u} x_i + 2(Ms - M\hat{s})^T M x_i \frac{\partial^2 s}{\partial u^2} x_j \quad (16)$$

B. Derivation on how to apply SBC to various Spiking ResNets and Spiking Transformer architectures

B.1. Spiking ResNets

Shortcut handling in Spiking ResNets We derive the SBC loss with surrogate membrane potential (SMP) for two popular Spiking ResNet variants: Spiking-Element-Wise (SEW) ResNet (Fang et al., 2021a) and SpikingResNet (Hu et al., 2023).

In SEW ResNet, the shortcut follows the spiking layer; from SBC’s perspective, the two branches are already independent modules and can be pruned separately.

In SpikingResNet, the shortcut precedes the spiking layer. Thus the external current to the next spiking layer is the sum of the convolution output and the shortcut output. Consider one neuron with linearized convolution output X_1w_1 , shortcut output X_2w_2 , and surrogate membrane-potential operator M . The shortcut loss is

$$L_{\text{shortcut}} = \mathbb{E}_X \left[\|M(X_1w_1 + X_2w_2) - M(X_1\hat{w}_1 + X_2\hat{w}_2)\|_2^2 \right] \quad (17)$$

$$= \mathbb{E}_X \left[\left\| M \left([X_1 \ X_2] \begin{bmatrix} w_1 \\ w_2 \end{bmatrix} \right) - M \left([X_1 \ X_2] \begin{bmatrix} \hat{w}_1 \\ \hat{w}_2 \end{bmatrix} \right) \right\|_2^2 \right]. \quad (18)$$

Hence we may concatenate the inputs and weights of the last convolution and the shortcut in each SpikingResNet block, forming a new module with input $X = [X_1 \ X_2]$ and weights $W = \begin{bmatrix} w_1 \\ w_2 \end{bmatrix}$. Compression is then performed on this module. If the shortcut has no trainable parameters, we simply mask out the weights associated with X_2 before compression. *Notation:* $[X_1 \ X_2]$ denotes horizontal concatenation; $\begin{bmatrix} w_1 \\ w_2 \end{bmatrix}$ denotes vertical concatenation.

B.2. Spiking Transformers

This section examines the applicability of **SBC** to popular *spiking-transformer* architectures, and we find that it extends cleanly to Spikformer (Zhou et al., 2022), Spikformer V2 (Zhou et al., 2024), and the Spike-Driven Transformer (SDT) (Yao et al., 2023).

Spikformer family. In Spikformer, the weights of the Spiking Self-Attention (SSA) layers (W_Q, W_K, W_V) belong to a Linear \rightarrow BN \rightarrow Spiking block and can therefore be treated as *three* SBC modules. Each MLP block follows Linear \rightarrow BN \rightarrow Spiking \rightarrow Linear \rightarrow BN \rightarrow Spiking, giving *two* additional modules. Spikformer V1 uses Spiking Patch Splitting (SPS), whereas V2 employs a Spiking Convolution Stem (SCS); both are sequential convolutions that fit the SBC module-wise compression definition in Section 3.

Spike-Driven Transformer (SDT). In SDT, the shortcut precedes the spiking layer, so the external current is the sum of the previous BN output and the shortcut. Let the main-path output be XW , the shortcut output U , and M the surrogate membrane-potential operator. For a single spiking layer, the shortcut loss is

$$\begin{aligned} L_{\text{shortcut}} &= \mathbb{E}_X \left[\|M(XW + U) - M(X\hat{W} + U)\|_2^2 \right] \\ &= \mathbb{E}_X \left[\|MXW + MU - MX\hat{W} - MU\|_2^2 \right] \\ &= \mathbb{E}_X \left[\|MXW - MX\hat{W}\|_2^2 \right]. \end{aligned} \quad (19)$$

Hence, the shortcut can be ignored during compression, allowing all SDT modules to be treated exactly as in Spikformer.

C. Experiment Implementation details

Note that we provide anonymised code for all experiments.

C.1. Static Models

We use the Spiking VGG16 model implemented by (Kim et al., 2022) for CIFAR100 experiments. We used the pre-trained SEW-ResNet and Spike-Driven Transformer families of models for our ImageNet pruning experiments.

C.2. Neuromorphic Models

The detailed architectures of the models applied to each neuromorphic dataset are given in the figures 4, 6, 5, 7. All LIF neuron layers use the surrogate function $Atan()$, time constant $\tau = 2.0$. Note the downsizing of CIFAR10-DVS dataset to 64x64, due to the computation limitation of our hardware.

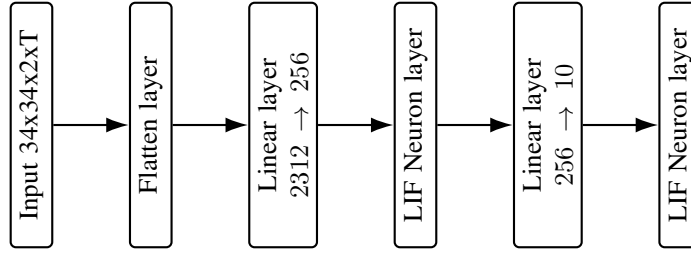


Figure 4. N-MNIST 2FC architecture

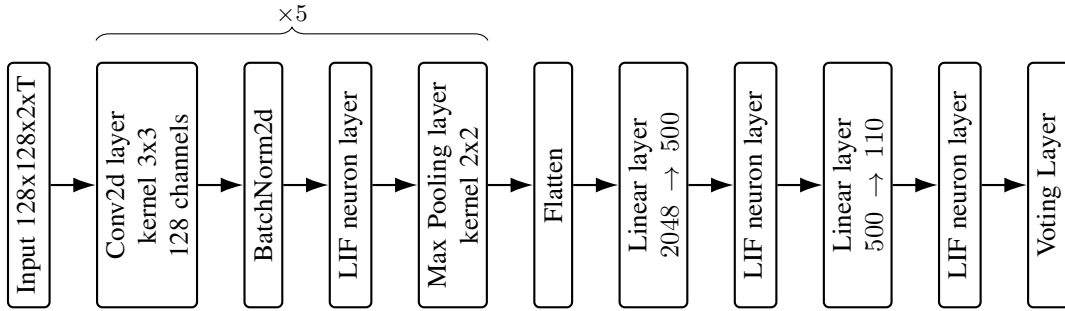


Figure 5. DVS128-Gesture 5Conv-2FC architecture

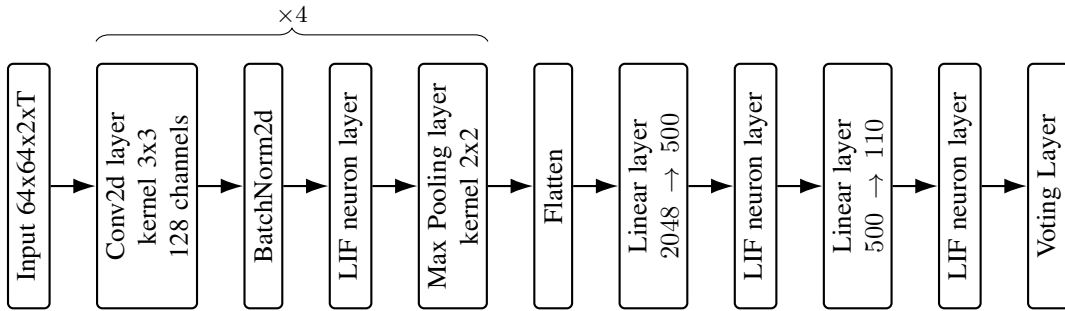


Figure 6. CIFAR10-DVS 4Conv-2FC architecture

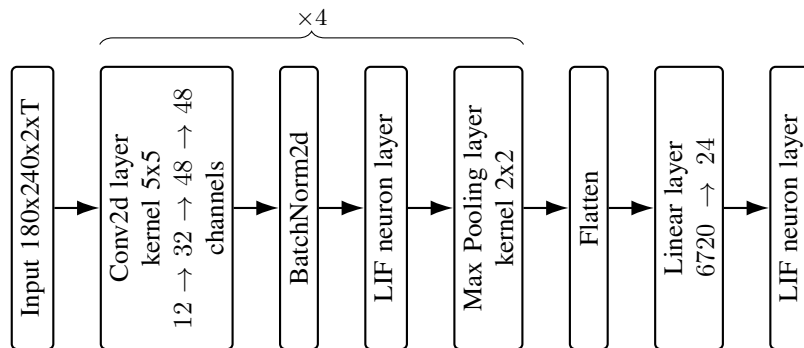


Figure 7. ASL-DVS 4Conv-1FC architecture

C.3. Pruning Experiments Details

The pruning percentage for each prunable layers in the module is pre-determined with LAMPS (Lee et al., 2020). Here is a summary:

LAMPS Let the weights of layer l be flattened into $\mathbf{W}^{(l)} \in \mathbb{R}^{N_l}$, and let π_l be the permutation that orders them in non-decreasing magnitude:

$$|W_{\pi_l(1)}^{(l)}| \leq |W_{\pi_l(2)}^{(l)}| \leq \dots \leq |W_{\pi_l(N_l)}^{(l)}|.$$

Then for $u = 1, \dots, N_l$, the *LAMP score* of the u -th smallest weight in layer l is

$$\text{LAMP}(l, \pi_l(u)) = \frac{(W_{\pi_l(u)}^{(l)})^2}{\sum_{v=u}^{N_l} (W_{\pi_l(v)}^{(l)})^2}. \quad (20)$$

To prune to a global sparsity level S , collect all scores $\{\text{LAMP}(l, \pi_l(u))\}$ across layers, and remove $\lfloor S \sum_l N_l \rfloor$ weights from each layer.

The weights in each module are then pruned in the order suggested by LAMPS scores; however, the exact weights pruned and compensations are determined by the SBC pruning algorithm. The exact implementation can be found in the supplementary file `osbc_prune.py`

C.4. Quantization

The quantization grid is chosen as a symmetric per-channel fixed-grid of width Δ_c . This means the maximum absolute value of a channel of weights equals the maximum value of the quantization grid. The symmetric quantization grid enables easy scalar conversion between compressed and original quantized values.

$$\hat{w}_c = w_{c_{quantized}} \times \Delta_c, w_{c_{quantized}} \in \{2^{n-1}, \dots, -1, 0, 1, \dots, 2^{n-1} - 1\} \quad (21)$$

For an n -bit quantization grid for channel c . The implementation of this maximum value grid is directly lifted from the GPTQ (Frantar et al., 2023) implementation on GitHub. It can be found in the supplementary file `quantizer.py`.

The quantization experiment was run five times at each quantization level, with five different seeds for the PyTorch and NumPy random number generators used to select a sample dataset from the training dataset. The exact seeds are available in `modelutils.py`. The implementation for OBSC quant can be found in `osbc_quant.py` in the supplementary material.

D. Experiment Result Tables

Table 5. Neuromorphic dataset pruning result

Setting	Method	Accuracy(%)					
		$p = 0\%$	80.00%	90.00%	95.00%	97.00%	98.00%
N-MNIST 2FC	LAMPS+MBP	98.31	65.39	29.40	35.13	26.94	25.60
	ExactOBS	98.31	98.16	98.01	96.91	91.59	53.24
	SBC(Ours)	98.31	98.13	98.10	97.63	96.72	93.97
CIFAR10-DVS 4Conv+2FC	LAMPS+MBP	71.50	69.70	65.70	29.10	10.90	10.00
	ExactOBS	71.50	70.50	67.50	58.40	36.60	20.70
	SBC(Ours)	71.50	71.50	69.40	66.40	61.30	49.80
DVS128-Gesture 5Conv+2FC	LAMPS+MBP	95.14	92.36	79.86	35.13	9.03	8.33
	ExactOBS	95.14	95.13	93.40	92.7	89.93	85.76
	SBC(Ours)	95.14	95.48	94.44	94.10	93.40	90.63
ASL-DVS 4Conv+1FC	LAMPS+MBP	96.53	88.11	36.48	11.76	7.19	6.08
	ExactOBS	96.53	95.51	93.41	87.52	77.23	62.78
	SBC(Ours)	96.53	95.73	93.72	89.12	81.40	70.30

Table 6. Static dataset pruning results: SBC vs. ExactOBS

Dataset	Arch.	Time step	Top-1 Acc. SBC(Ours) (%)	Top-1 Acc. ExactOBS (%)	Weight Sparsity (%)	Time (h) A4500 Eq.	Calib. size (% train)
CIFAR100	VGG16-SNN	5	71.40	71.40	0	-	-
			70.63	70.63	68.30	0.21	20%
			66.44	65.89	89.91	0.20	20%
			48.93	41.46	95.69	0.20	20%
ImageNet	SEW-ResNet18	4	63.18	63.18	0	-	-
			62.61	62.49	50.00	0.208	2%
			61.03	60.71	66.67	0.214	2%
			58.94	57.34	75.00	0.220	2%
	SEW-ResNet50 [†]	4	67.78	67.78	0	-	-
			66.88	66.75	50.00	0.346	2%
			63.86	62.97	66.67	0.344	2%
			58.50	55.50	75.00	0.341	2%
SEW-ResNet152 [†]	4	69.26	69.26	0	-	-	
		67.88	67.88	50.00	0.783	2%	
		62.53	61.06	66.67	0.808	2%	
			51.30	46.19	75.00	0.723	2%

* **Bolded** entries represent best accuracies in sparsity class

[†] Deepest SNN models pruned to date. No existing PAT methods have pruned them.

Table 7. Static dataset pruning results, SBC compared with Pruning-Aware-Training methods

Dataset / Model	Time step	Pruning Method	Top-1 Acc. (%)	Weight Sparsity (%)	Time (h) A4500 Eq.	Calib. size (% train)	Finetune epochs
CIFAR100 VGG16- SNN	5	LTH IMP	69.08	68.30	15.23	–	–
			68.90	89.91	27.22	–	–
			68.00	95.69	36.22	–	–
		LTH EB	67.35	68.30	3.44	–	–
			65.82	89.91	4.36	–	–
			61.90	95.69	5.24	–	–
	SBC (Ours)	70.63	68.30	0.21	20%	–	
		66.44	89.91	0.20	20%	–	
		48.93	95.69	0.20	20%	–	
	SBC + Finetune	71.10(+0.47†)	68.30	0.51	20%	25.0	
		68.96(+2.52†)	89.91	0.81	20%	50.0	
		63.34(+14.41†)	95.69	0.81	20%	50.0	
ImageNet SEW- ResNet18	4	STDS	61.51	65.21	180	–	–
			61.30	70.71	180	–	–
			59.93	78.92	180	–	–
		UPF	61.89	64.74	125	–	–
			60.00	72.26	118	–	–
			SBC (Ours)	61.36	64.74	0.208	2%
	60.31	70.71		0.213	2%	–	
	59.86	72.26		0.220	2%	–	
	56.48	78.92	0.220	2%	–		
		SBC + Finetune	61.90(+0.54†)	64.74	12.00	2%	5.0
			60.82(+0.51†)	70.71	2.75	2%	1.0
	60.38(+0.52†)		72.26	2.75	2%	1.0	
58.46(+1.98†)	78.92	2.75	2%	1.0			

* **Bolded** entries represent best accuracies/shortest compression time in sparsity class

† Accuracy improvements compared to pre-finetuned, SBC pruned models

Table 8. ImageNet pruning on Spike-Driven Transformer: SBC vs. ExactOBS

Dataset	Arch.	Time step	Top-1 Acc. SBC (Ours) (%)	Top-1 Acc. ExactOBS (%)	Weight Sparsity (%)	Time (h) A4500 Eq.	Calib. size (% train)
ImageNet	SDT 6_512	4	73.89	73.89	0.00	–	–
			71.88	71.68	50.00	0.212	1%
			64.27	63.40	66.67	0.204	1%
			50.91	49.31	75.00	0.206	1%

* **Bolded** entries represent best accuracies in each sparsity class.